JOURNAL OF GEOPHYSICAL RESEARCH, VOL. 117, C09027, doi:10.1029/2012JC008182, 2012

Along-shelf current variability on the Catalan inner-shelf (NW Mediterranean)

Manel Grifoll,[1,2] Alfredo L. Aretxabaleta,[3] Manuel Espino,[1,2] and John C. Warner[3]

Received 8 May 2012; revised 30 July 2012; accepted 14 August 2012; published 22 September 2012.

[1] We examine the circulation over the inner-shelf of the Catalan Sea using observations of currents obtained from three Acoustic Doppler Current Profilers (two at 24 m and one at 50 m) during March–April 2011. The along-shelf current fluctuations during that period are mainly controlled by local wind stress on short time scales and by remote pressure gradients on synoptic time scales. Different forcing mechanisms are involved in the along-shelf momentum balance. During storm conditions, wind stress, sea level gradients and the nonlinear terms dominate the balance. During weak wind conditions, the momentum balance is controlled by the pressure gradient, while during periods of moderate wind in the presence of considerable stratification, the balance is established between the Coriolis and wind stress terms. Vertical variations of velocity are affected by the strong observed density gradient. The increased vertical shear is accompanied by the development of stratified conditions due to local heating when the wind is not able to counteract (and break) stratification. The occasional influence of the Besòs River plume is observed in time scales of hours to days in a limited area in near the city of Barcelona. The area affected by the plume depends on the vertical extent of the fresher layer, the fast river discharge peak, and the relaxation of cross-shore velocities after northeast storm events. This contribution provides a first interpretation of the inner-shelf dynamics in the Catalan Sea.

Citation: Grifoll, M., A. L. Aretxabaleta, M. Espino, and J. C. Warner (2012), Along-shelf current variability on the Catalan inner-shelf (NW Mediterranean), *J. Geophys. Res.*, *117*, C09027, doi:10.1029/2012JC008182.

1. Introduction

[2] The inner continental shelf is the transition zone between the surf zone (or nearshore zone), a region dominated by the wind-wave breaking process, and the mid-shelf, where the frictional layers (bottom and surface) are separated. The dynamics over the inner-shelf can contain elements of surf zone and mid-shelf processes, resulting in increasingly complex dynamics. Several studies describe a wide range of non-negligible driving mechanisms over the inner-shelf as a function of depth [*Allen and Kundu*, 1978; *Lentz*, 1994; *Li and Weisberg*, 1999; *Fewings and Lentz*, 2010]. For instance, *Lentz et al.* [1999] characterize three dynamically distinct regions in the range of 4 to 30 m depths identified by different dominant across-shelf momentum balance. Over the inner-shelf, the balance tends to be between pressure gradient and frictional (bottom and wind stress) forces in the along-shelf [*Lee et al.*, 1984; *Lentz and Winant*, 1986; *Lentz*, 1994; *Fewings and Lentz*, 2010]. A strong temporal variability in the along-shelf direction can also be present as a function of upwelling favorable/unfavorable winds [*Kirincich and Barth*, 2009].

[3] In the present study, the dynamics over the inner-shelf of the Catalan Sea (NW Mediterranean Sea) are examined using a set of observations from a field campaign during spring 2011. The area of study extends from 41.37°N to 41.43°N and from 2.19°E to 2.28°E (Figure 1). This area is located offshore of the northeastern districts of Barcelona City (between the north mouth of the harbor and the Besòs River mouth). Near-inertial motions, associated with active wind events, are the dominant fluctuations over the shelf and slope of the Catalan Sea [*Salat et al.*, 1992; *Rippeth et al.*, 2002]. A southwestward flow due to the influence of the quasi-permanent Northern Current [*Millot*, 1999] has been described over the slope with lower density water being found onshore of the current [*Salat et al.*, 1992]. The Northern Current is in geostrophic equilibrium with a shelf/slope density front, with the surface signature of the front located between 28 km and 55 km offshore [*Rubio et al.*, 2005]. Using circulation model simulations, *Jordà and De Mey* [2010] found consid-

[1]Laboratori d'Enginyeria Marítima, Universitat Politècnica de Catalunya, Barcelona, Spain.
[2]Centre Internacional d'Investigació dels Recursos Costaners, Barcelona, Spain.
[3]U.S. Geological Survey, Woods Hole, Massachusetts, USA.

Corresponding author: M. Grifoll, Laboratori d'Enginyeria Marítima, Universitat Politècnica de Catalunya, Campus Nord, c./ Jordi Girona, 1-3, ES-08034 Barcelona, Spain. (manel.grifoll@upc.edu)

0148-0227/12/2012JC008182

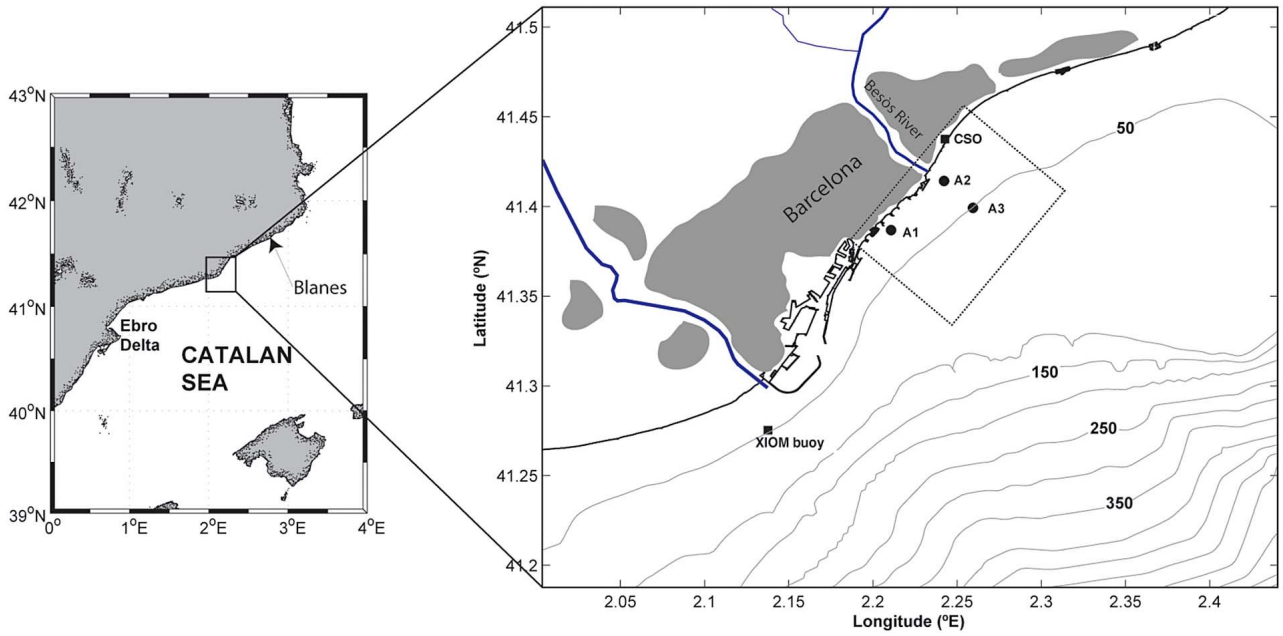

Figure 1. Map of the Catalan Sea and (inset) bathymetry of a portion of the Catalan inner-shelf showing sensor locations. The geographical locations mentioned in the text and the study area (dotted rectangle) are also shown.

erable meso-scale activity (eddies, filaments, and meanders) over the slope and outer shelf region. The mid- and outer Catalan shelf was conceptually analyzed by *Sánchez-Arcilla and Simpson* [2002] at south of our study area in a region strongly influenced by the freshwater outflow of the Ebro River (south margin of the Catalan Sea; see Figure 1). *Salat et al.* [2002] analyzed the seasonal exchanges in the shelf-slope in the same Ebro River area. In summary, the central part of the Catalan inner-shelf remains poorly understood because of the lack of systematic observational or model studies.

[4] The study area, as many parts of the Mediterranean environment, is under strong anthropogenic pressure and requires in-depth knowledge of the marine environment for appropriate management. The part of the Catalan shelf under study exhibits micro-tidal fluctuations and is relatively narrow. Catalan shelf widths are between 20 km in the observation area and 60 km in the south margin near the Ebro Delta. The shelf break is approximately located at the 150 m isobath and the averaged slope is of the order of 10^{-2}. The wind regime is characterized by small inter-annual variability [*Font*, 1990]. The predominant winds come from the north and northwest, primarily during fall and winter, where its energy concentrated in low frequencies (periods over 3 days) associated with synoptic low-pressure systems [*Salat et al.*, 1992]. In summer and spring, the dominant winds are south-westerly, with the dominant frequencies being the synoptic and diurnal (sea-breeze) bands [*Font*, 1990].

[5] The goal of this paper is to provide a dynamic description of the main physical processes over the inner Catalan shelf by using a set of observations (section 2) through thorough statistical analysis (section 3). The main results (section 4) are the description of the relation between flow observations and driving mechanisms, the estimation of the momentum balance terms, and the analysis of the stratification and baroclinic process. In section 5, we underline the main conclusions and propose open questions for future work.

2. Observations

[6] The bulk of the measurements correspond to a field campaign conducted during March and April 2011 over the Catalan inner-shelf in the framework of the FIELD_AC project (www.field_ac.eu). The data set consists of water velocity time series from three Acoustic Doppler Current Profiler (ADCP) deployments (A1 [AWAC], A2 [AWAC] and A3 [RDI], Figure 1). The bin size in the ADCPs is 1 m. The along-shore distance between A1 and A2 was 4 km. A1 and A2 were deployed approximately less than 1 km from the coast (at 24 m depth) while A3 was 2 km away from the coast (at 50 m depth). Wind data were collected using a mast located at a Coastal Station Observatory (www.pontdelpetroli.org) and a wave buoy that is part of the XIOM network (www.xiom.cat) located 17 km from the field campaign area (Figure 1). In addition, 43 CTD profiles were collected on March 17 and another 42 profiles April 10 on the area surrounding the ADCPs. Besòs River runoff data were obtained from a monitoring station upstream of the river mouth (www.aca.cat). The March 17 CTD survey corresponds to "post-rain conditions" associated with a short and intense Besòs River discharge of 50 m^3s^{-1} (mean flow conditions are 4 m^3s^{-1}). These "flash-flood" conditions occur during short (hours to days of duration) and intense

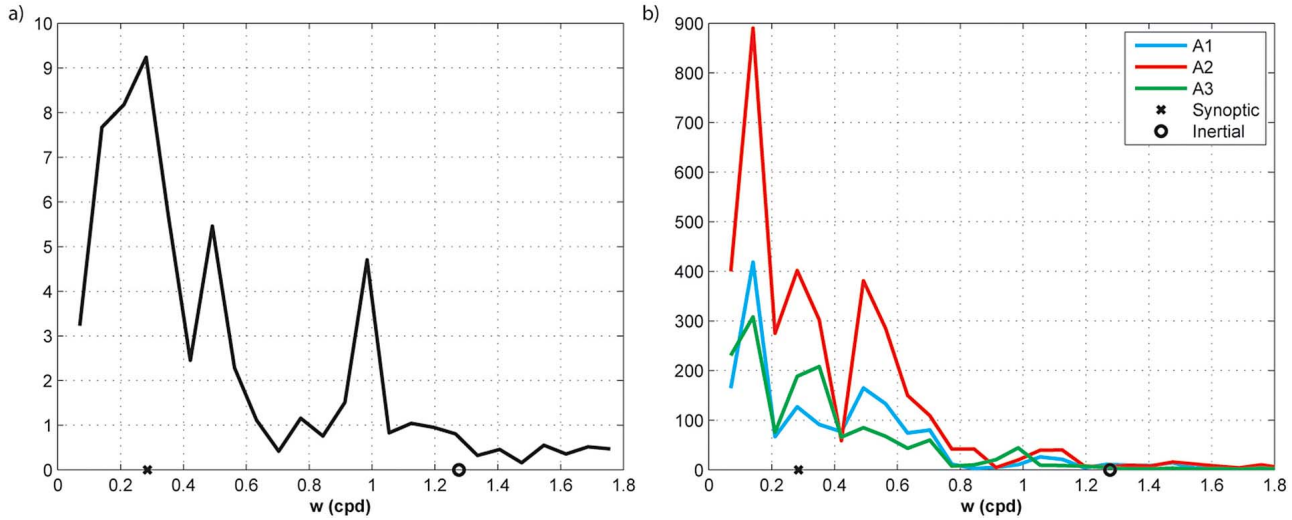

Figure 2. Along-shelf power spectra (m^2/s) for (a) the along-shelf measured wind and (b) the three ADCP along-shelf velocities. Synoptic and inertial frequencies are also shown.

storm events, typical of the Mediterranean climate, in small river mountainous drainage basins [*Bourrin et al.*, 2008].

3. Data Description and Results

3.1. Wind Measurements

[7] Typical wind directions observed during the field campaign are northeasterly, southwesterly and onshore/offshore. The strongest wind intensities were associated with northeasterly winds (11 m s^{-1}). The power spectrum of the along-shelf wind (Figure 2a) reveals a large peak concentrated at low frequencies (periods over 3 days) with a smaller peak associated with sea breeze (period of ~1 day) that is common in the Northwestern Mediterranean during spring [*Font*, 1990]. The low-frequency energy is associated with the synoptic passage of low-pressure systems, which in the Catalan Sea corresponds to 3–12 days [*Font*, 1990]. The comparison of the wind from the two previously mentioned meteorological stations exhibits only small differences (with correlations of R = 0.89 for the east-west component and R = 0.75 for the north-south component). Consequently, we assume the time series from the coastal station is representative of the study area. Wind velocities are converted to stress following the neutral drag law [*Large and Pond*, 1981].

3.2. Hydrography

[8] Surface temperature and salinity during the two sampling periods (CTD1, March 17 and CTD2, April 10) are presented in Figure 3. The surface salinity exhibits larger spatial variability in CTD1 (post-rain conditions) due to the presence of the signal of Besòs River freshwater (see river discharge in Figure 3a). The plume signal is constrained to the first few meters of the water column in the CTD section perpendicular to the coast at the river mouth. During the CTD2 survey (normal conditions), the influence of the plume is small and localized at the river mouth, resulting in fairly constant horizontal temperature and salinity structure. The river plume signal is identified in the density section offshore of the river mouth (Figures 3f and 3g).

[9] The water column is stratified in both surveys. The buoyancy (Brunt-Väissälä) frequency (N) for the averaged profile is shown in Figures 4a and 4b. While both buoyancy frequency profiles exhibit significant stratification, during post-rain conditions (CTD1) the stratification is concentrated in the shallow layers (0–4 m depth) due to the low-salinity river plume. N decreases from $6{\cdot}10^{-2}$ s^{-1} in the surface layers to 10^{-2} s^{-1} in the subsurface and bottom layers (well-mixed conditions below surface layer) during CTD1. The normal conditions (CTD2) also present a stratified profile but now maximum frequencies (N = 0.04 s^{-1}) are at 5 and 12 m. Vertical profiles of density (Figure 4c) demonstrate equal contributions from salinity and temperature except in the surface layer, where the temperature has a predominant effect in the density profile. The density gradient is ~0.05 kg m^{-2}, increasing in depth.

3.3. Observations of Currents

[10] The observed currents at the three sites (A1, A2, and A3) are strongly polarized in the along-shelf direction (Figure 5) with a maximum speed of 60 cm s^{-1} at A2. The major axis of the variance ellipses accounts for 80% of the variability of the flow in all ADCPs. Basic statistics are presented in Table 1. Using the angle of the principal axis, the angle of maximum variance is found to be similar to the coastline orientation. Standard deviations in the along-shelf direction, given by the major axis of the ellipse, are between 2 and 6 times larger than cross-shelf current standard deviations (minor axis). For the analysis in the along-shelf direction, the coordinate system is rotated so that the y-component corresponds to the velocities in the along-shelf direction (see Figure 5). The *y* axis is different for each mooring as it matches the principal axis of variation. Along-shore net currents are southwestward and the magnitude is between 3 and 10 cm s^{-1} (Table 1).

[11] The average currents at A1 are larger than those observed at A2 and A3. Vertical differences in the horizontal velocity are also observed in the measurements (Table 1). The maximum vertical difference in along-shore velocities

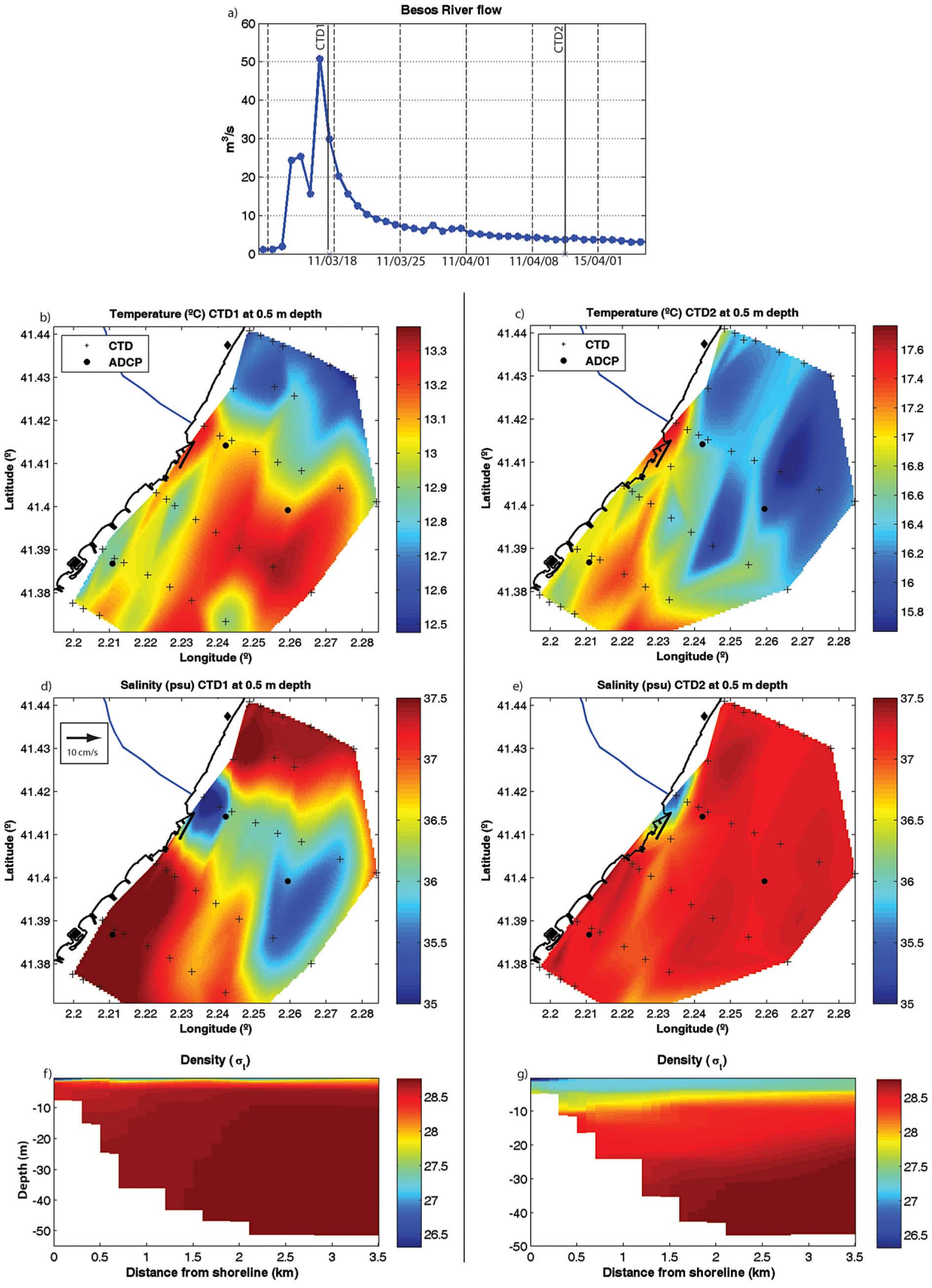
a)
Besos River flow
m3/s
CTD1
CTD2
11/03/18
11/03/25
11/04/01
11/04/08
15/04/01
b)
Temperature (ºC) CTD1 at 0.5 m depth
c)
Temperature (ºC) CTD2 at 0.5 m depth
CTD
ADCP
d)
Salinity (psu) CTD1 at 0.5 m depth
e)
Salinity (psu) CTD2 at 0.5 m depth
10 cm/s
Latitude (º)
Longitude (º)
f)
Density (σt)
g)
Density (σt)
Depth (m)
Distance from shoreline (km)

Figure 3

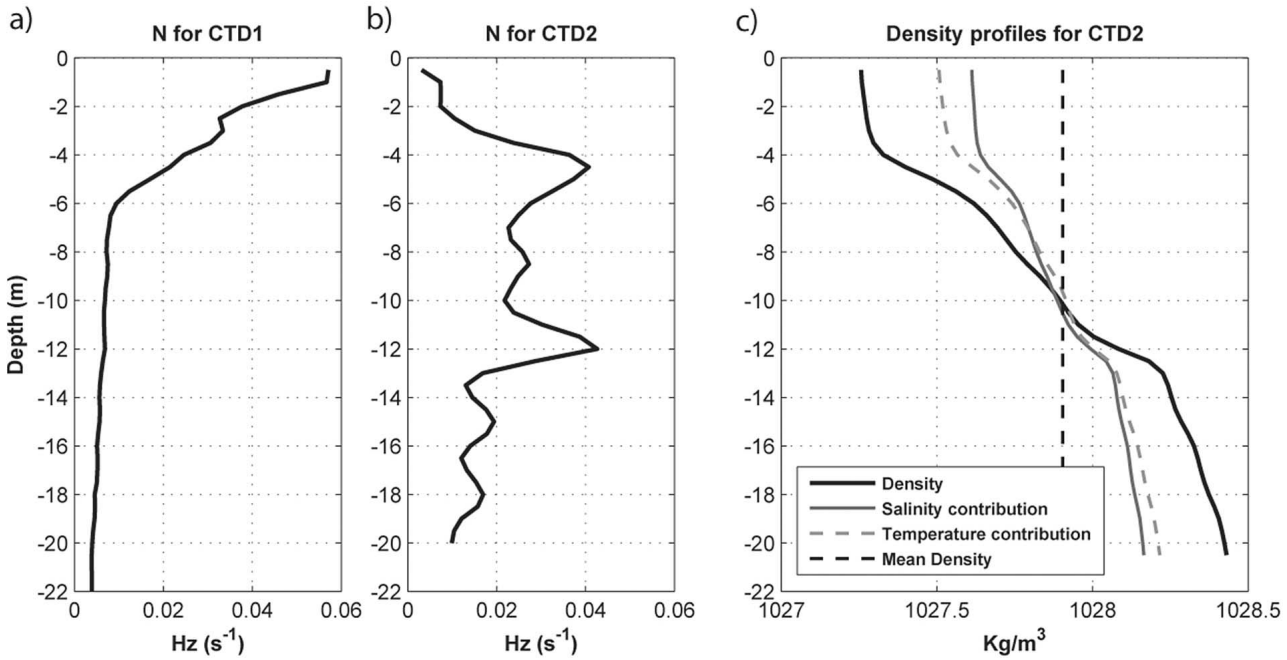

Figure 4. Buoyancy frequencies computed from the density profiles for the (a) CTD1 and (b) CTD2. The stations used correspond to the section in front of Besòs River mouth. (c) Section-averaged density profile (during CTD2, April 10) at the 22 m isobath and temperature and salinity contributions to the density profile. The temperature (salinity) contribution to the density profile has been calculated using the observed temperature (salinity) profile while assuming a constant salinity (temperature) to calculate density.

is 20 cm s^{-1}, with the surface layer generally being more energetic than the deeper layers. The largest mean velocity vertical difference in the along-shore direction is measured at the deepest ADCP (A3) with mean values of 6 cm s^{-1}. The mean values for A2 and A1 are around 2 cm s^{-1}. The standard deviations in all cases are of the order of 10 cm s^{-1}. The correlations between the velocity time series measured at different locations range from 0.84 to 0.92.

[12] An Empirical Orthogonal Function (EOF) analysis of the along-shelf velocity time series identifies 90% of the current variance as being accounted for by the first two modes. The largest EOF accounts for 77% of the total current variance in A1 and 82% in A2 and A3. The first mode is highly correlated with the depth-averaged along-shelf currents (correlation larger than 0.95).

[13] The vertical structure of the three principal modes is shown in Figure 6. The first mode shows a vertical shear that we associate with barotropic fluctuations (we call barotropic the modal structure which does not reverse with depth as in *Winant and Bratkovich* [1981]) with near-bottom magnitude being smaller than surface values. The second mode accounts for 10% of the flow variance approximately. The second and third modes exhibit an inversion throughout the water column.

[14] To identify the dominant frequency of the flow, spectral analysis is conducted on the depth-averaged along-shore currents at each ADCP. The power spectra (Figure 2b) reveals that low frequency current variability is important similarly to what was observed for the wind. Highly energetic bands in the along-shelf currents are found below 0.6 cpd, associated with synoptic fluctuations lasting 3–12 days in the Northwestern Mediterranean Sea [*Font*, 1990]. Diurnal and inertial (1.29 cpd) frequency bands, which were the dominant motions over the slope [*Font*, 1990; *Salat et al.*, 1992], are comparably small.

4. Analysis and Discussion

4.1. Along-Shore Velocity Response

[15] The dynamics in the inner-shelf are influenced by the proximity of the coastal boundary layer that slows down the flow across to shelf. This is one of the most important constraints in inner-shelf dynamics resulting in the along-shelf flow being predominant in comparison to the cross-shelf [*Pettigrew and Murray*, 1986]. In our case, the influence of the coastal boundary layer is appreciated in the measurements as a velocity adjustment due to the presence of the shore resulting in an along-isobath flow (Figure 5).

[16] Shallow areas promote frictional influences in the flow (bed-shear and wind stresses) due to the fact that the water depth is comparable to the thickness of the Ekman layers [*Allen and Kundu*, 1978]. This can lead to strong correlations

Figure 3. (a) Time series of the Besòs River discharge. The time of the two CTD survey is shown with vertical solid line. (b and c) Temperature and (d and e) salinity for the surface layer for (left) CTD1 and (right) CTD2. In the contour plots the CTD survey stations are marked with a cross and the ADCP locations with a solid circle. Density sections in front of the Besòs mouth for (f) CTD1 and (g) CTD2.

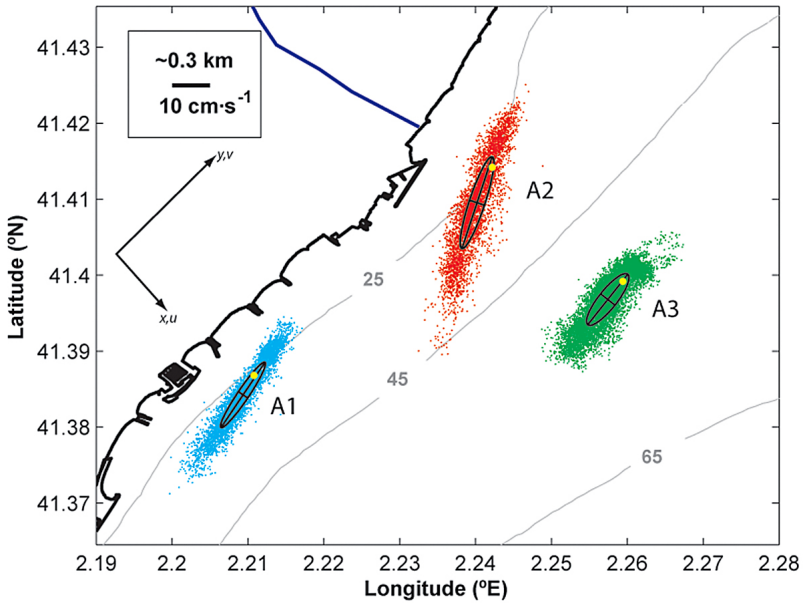

Figure 5. Dispersion diagram and variance ellipses computed from depth-averaged ADCP measurements. The mooring location of each ADCP is marked with a yellow circle. The distance between the circle and the center of each ellipse represents mean velocity. The minor and the major sub-axes correspond to the standard deviation. The rotated axis with the associated velocity components x, u and y, v represents the adopted reference system for the momentum balance.

between wind and along-shelf currents. In the Catalan inner-shelf during the period analyzed, the correlations are between 0.35 and 0.57 suggesting that the flow can be explained up to 50% by the local wind-forcing. The influence of local wind in shelf motions has been widely reported [*Winant and Beardsley*, 1979; *Li and Weisberg*, 1999; *Fewings and Lentz*, 2010]. Despite the high correlations, the local wind only provides partial explanation of the flow fluctuations.

[17] Another factor to consider is the pressure gradient given by the free surface elevation in the along-shelf. This pressure gradient can be an important forcing even when the water depth is comparable to the Ekman layer depth [*Lee et al.*, 1984; *Lentz and Winant*, 1986; *Sánchez et al.*, 2006]. In our case, the sea level gradient is estimated using data from a sea level gauge located in Blanes Harbor and the ADCP pressure sensor at A2 (approximately 64 km apart, Figure 1). Considering the reference axis for the along-shelf (y) shown in Figure 5, positive sea level gradients correspond to higher sea level in Blanes than at the ADCP. The sea level time series in Blanes Harbor, strongly influenced by local effects, is adjusted using daily sea level variations from MyOcean model outputs (www.myocean.eu), which assimilate Sea Level Anomaly from satellite altimetry and have been corrected for atmospheric pressure [*Tonani et al.*, 2009]. This adjustment also helps approximate the sea level decay from the coast to the inner-shelf associated with coastal trapping [*Hickey*, 1984; *Liu and Weisberg*, 2005]. Correlations between sea level gradient and depth-averaged along-shore currents can be of the same order as correlations with local wind (e.g., R = −0.43 during some events). The negative value of this correlation is consistent with the current

Table 1. Basic Statistics of the ADCP Along-Shore Currents

	Depth (m)	Principal Axis Orientation (deg)	Mean Along-Shelf (cm/s)	Std. Dev. Along-Shelf (cm/s)	Variability of Along-Shelf
A1	−1	56°	−4.08	14.80	89%
	−12	52°	−6.19	10.94	86%
	−24	61°	−3.23	6.50	78%
	Depth-averaged	**56°**	**−5.25**	**9.61**	**98%**
A2	−1	26°	−8.94	20.27	85%
	−12	18°	−10.43	13.54	92%
	−24	14°	−6.54	9.00	86%
	Depth-averaged	**18°**	**−10.08**	**12.73**	**97%**
A3	−2	40°	−8.78	12.96	86%
	−25	40°	−6.13	8.71	84%
	−47	40°	−2.78	8.29	86%
	Depth-averaged	**39°**	**−6.20**	**8.48**	**94%**

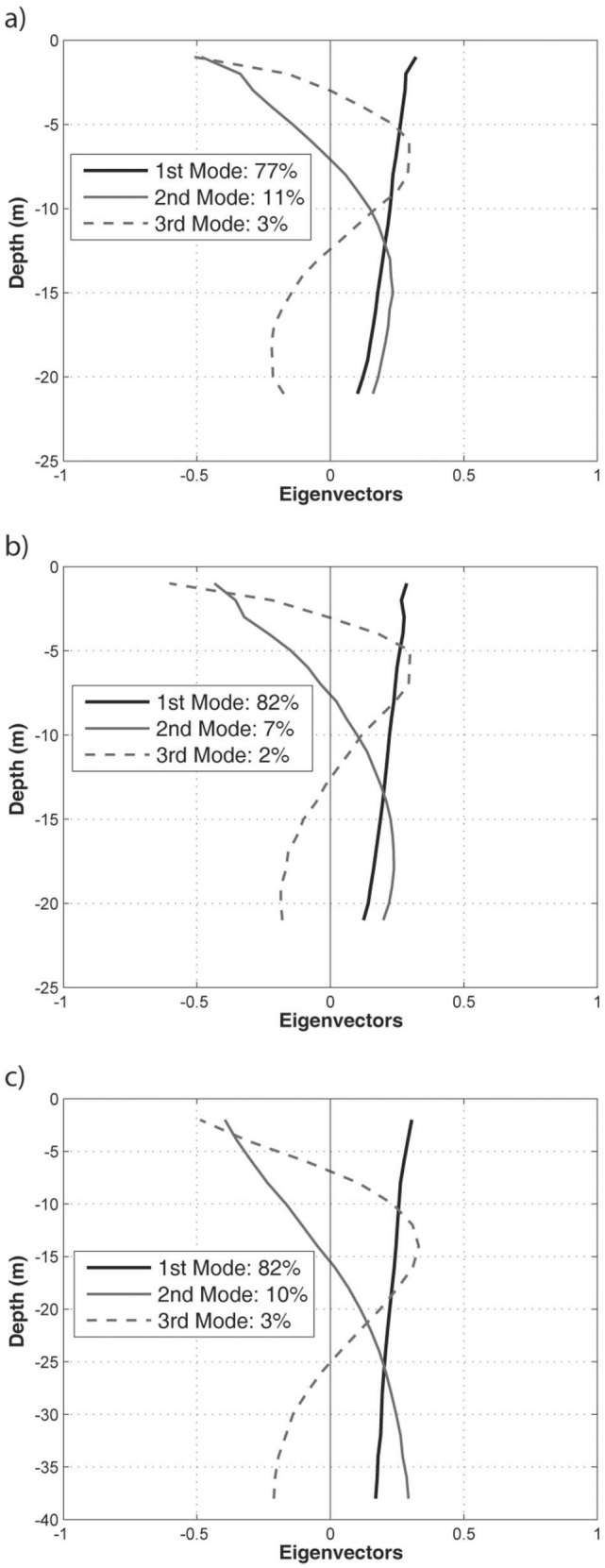

Figure 6. Vertical profiles and explained variances (in the legend) of the first modes of variability for (a) A1, (b) A2 and (c) A3 along-shelf velocities.

response to sea level adjustments observed in shelf dynamics [*Hickey*, 1984].

[18] To understand the relationship between winds, pressure gradient and water flow, a descriptive analysis of the corresponding time series is conducted. The filtered (f_c = 2 cpd) time series of local wind, sea level gradient and along-shelf currents (Figure 7) identify three different regimes: northeasterly winds, weak local winds, and southwesterly winds.

[19] The first regime is associated with a northeasterly wind event (12–15 March with 0.15 N m^{-2} maximum stress, blue bar in Figure 7). During this period, the wind stress generates a negative sea level gradient. The water response is flow toward the southwest with depth-averaged along-shore currents of the order of 30 cm s^{-1}. During this event the along-shore current measurements are positively correlated with the wind stress and the sea level gradient (R = 0.83 and R = 0.74, respectively).

[20] Another distinctive regime, repeated several times during the period of analysis, is characterized by weak local winds and a relative strong sea level gradient that can be positive or negative (red bars in Figure 7). During this regime, when the sea level gradient is positive, the water flows along-shore toward southwest, resulting in negative correlations. Speeds vary during different events with maximum magnitudes above 30 cm s^{-1}. The positive sea level gradient is associated at least partially with the general dynamics of the NW Mediterranean Sea presumably related with the regional response to forcing and bathymetry in the Catalan inner-shelf. This larger-scale gradient is consistent with the Northern Current that follows the continental slope in the Northwest Mediterranean Sea [*Millot*, 1999]. Conversely, the regime contains occurrences of weak winds with a negative sea level gradient as observed during 4–8 April. In this case, the current direction switches to northeastward and is presumably associated with the excursion of water from the south that follows the coast toward the north forced by a negative pressure gradient. These water masses, perhaps influenced by inflow of Atlantic water into the Mediterranean or strongly modified by local fresh inputs, may be identified in the onshore side of the slope front in the Catalan Sea [*Salat et al.*, 2002].

[21] A third regime is associated with short periods of southeasterly wind reversing the flow toward the northeast (yellow bars in Figure 7). During these events, the local wind pushes water toward the northeast in the along-shelf direction with peaks of 15 cm s^{-1}. During this regime, a well-defined faster response to the forcing is observed in the flow.

[22] In summary, the along-shelf flow patterns are caused by two main forcing factors: 1) wind events associated with fast flow response, and 2) remote sea level gradients with temporal scales of several days (synoptic) consistent with the spectral analysis. The separation between the two sea level stations (64 km) is enough to capture the barotropic signal of the sea level gradient, considering that over the Catalan shelf the external Rossby radius of deformation is around 100 km [*Sánchez-Arcilla and Simpson*, 2002]. As a consequence, the correlation between the measured sea level gradient and local wind is small. During storm events, a combination of both forcings (wind and pressure gradient) is also found interacting and reducing the temporal and spatial scales.

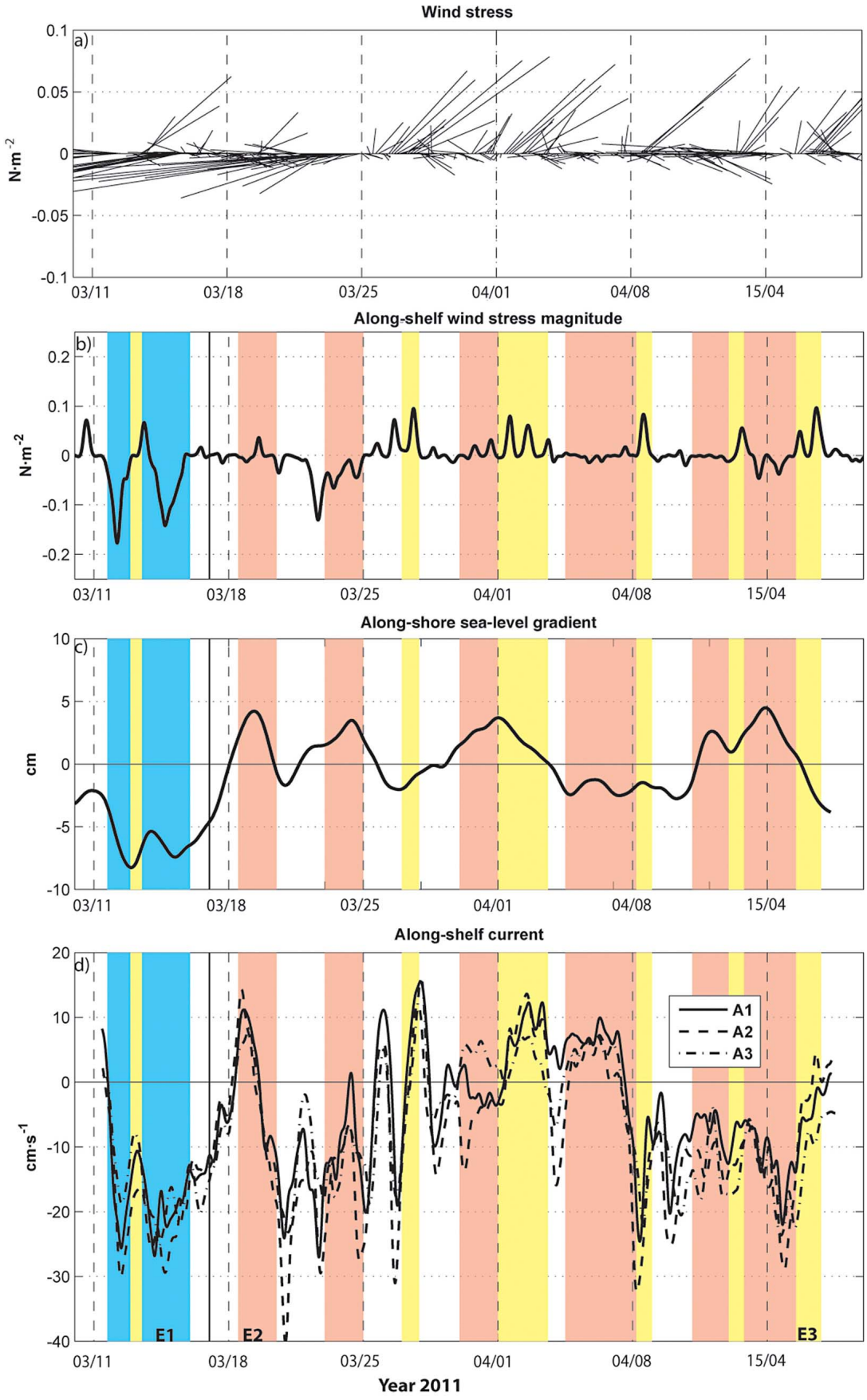
Wind stress
a)
N·m-2
0.1
0.05
0
-0.05
-0.1
03/11
03/18
03/25
04/01
04/08
15/04
Along-shelf wind stress magnitude
b)
N·m-2
0.2
0.1
0
-0.1
-0.2
Along-shore sea-level gradient
c)
cm
10
5
0
-5
-10
Along-shelf current
d)
cm·s-1
20
10
0
-10
-20
-30
-40
A1
A2
A3
E1
E2
E3
Year 2011

Figure 7

Table 2. Estimated Mean Momentum Balance Terms for the Depth-Averaged Along-Shelf Current (Units $\times 10^{-6}$ m s^{-2}) in A2 for the Different Episodes Analyzed

Episode	Period	$\frac{\partial \overline{v}}{\partial t}$	$\frac{\partial \overline{v}^2}{\partial y}$	$\frac{\partial \overline{uv}}{\partial x}$	$f\overline{u}$	$= -g\frac{\partial \eta}{\partial y}$	$-\frac{g}{H\rho_0}\frac{\partial}{\partial y}\int_{-h}^{\eta} g\rho z dz$	$\frac{\tau_{ys}}{H\rho_0}$	$\frac{\tau_{yb}}{H\rho_0}$
E1	Storm peak 12 March	0.13	[±5]	[±0.8]	−0.12	6.78	−0.65	−9.32	1.78
E2	19–21 March	−2.61	[±5]	[±0.9]	−0.65	−3.38	−0.45	0.16	0.75
E3	16–17 April	1.81	[±0]	[±3]	−1.24	−0.61	−0.45	2.07	0.25

Based on the observed forcing mechanisms, a first estimate of the momentum balance in the inner-shelf would be primarily between acceleration, wind stress and pressure gradient, similar to observational studies presented by *Hickey* [1984], *Lee et al.* [1984], and *Lentz and Winant* [1986]. The specifics of the dynamic balance will be analyzed and corroborated in the following subsection.

[23] The absence of flow in near-inertial frequencies that had been described in the south margin of the outer-shelf and slope (165 m depth) of the Catalan Sea [*Font*, 1990] is related to the depth constraint over the inner-shelf that shifts the energy organization of the flow. In our case, inertial oscillations do not appear presumably due to the "coastal constraint" [*Pettigrew and Murray*, 1986] and the fact that there is not enough depth to develop inertial motions because of the frictional effects (both bottom and surface Ekman layer thicknesses are of the same order as the water depth).

4.2. Along-Shore Momentum Balance

[24] Several mechanisms contributing to flow variability have not been included in the presented analysis. Factors such as nonlinear effects, local/spatial wind variability, or the presence of meso-scale activity [*Jordà and De Mey*, 2010; *Salat et al.*, 1992] can significantly alter the flow and complicate the interpretation of its variability.

[25] To better understand the dynamic response within the inner-shelf, the depth-averaged momentum terms are estimated at the A2 location. The along-shelf depth-averaged flow evolution equation (assuming no wave-current interactions) is:

$$\frac{\partial \overline{v}}{\partial t} + \frac{\partial \overline{v}^2}{\partial y} + \frac{\partial \overline{u}\overline{v}}{\partial x} + f\overline{u} = \frac{\partial \overline{p}}{\partial y} + \frac{\tau_{ys}}{H\rho_0} - \frac{\tau_{yb}}{H\rho_0} \quad (1)$$

where overbar denotes a depth-averaging:

$$(\bar{}) = \frac{1}{H}\int_{-h}^{\eta} () dz$$

[26] $H = \eta + h$ is the total depth, ρ_0 the reference density, and z is the vertical coordinate positive upwards from mean sea level at z = 0.

[27] The first term of the left hand side ("response") of equation (2) is the acceleration. The second and third terms correspond to the nonlinear advective terms. The fourth term corresponds to the Coriolis term and is computed considering the across-shelf fluxes ($f = 9.6 \cdot 10^{-5}$ s^{-1}).

[28] The nonlinear terms are difficult to estimate using observations because the spatial description of the flow is strongly simplified. An approximation of the size of the nonlinear terms was presented by *Lentz and Chapman* [2004] and applied in the along-shore balance by *Kirincich and Barth* [2009], where they used finite differentiation between ADCP measurements. Following their methodology, the across-shelf advection term $(\partial \overline{uv}/\partial x)$ can be estimated between A2 and A3 and the along-shelf advection term $\left(\partial \overline{v}^2/\partial y\right)$ is estimated from the differences between A1 and A2.

[29] The right side of the equation (2) ("forcings") includes three terms. The first term is the total along-shelf pressure gradient and can be computed as the contribution of the sea level slope (barotropic term) and the depth averaged water column (baroclinic term) according to the following equation:

$$\frac{\partial \overline{p}}{\partial y} = -g\frac{\partial \eta}{\partial y} - \frac{g}{H\rho_0}\frac{\partial}{\partial y}\int_{-h}^{\eta} g\rho z dz \quad (2)$$

where ρ is the density.

[30] The barotropic term is estimated using the previously computed sea level difference divided by the distance between the sea level gauge and the pressure meter (64 km). The baroclinic term has been calculated using the two most distant sections of the CTD survey. The value of this term might not be extended to the entire period but the estimate using CTD1 and CTD2 measurements provides an idea of its magnitude. Finally, the frictional terms are the second and third terms of the right hand side of equation (1) and correspond to wind (τ_{ys}) and bottom stress (τ_{yb}). To estimate the bottom stress at each site a quadratic drag formula is also used:

$$\overrightarrow{\tau_{yb}} = \rho_0 C_D |\overrightarrow{u_b}| u_b \quad (3)$$

where u_b is the observed velocity above the bottom (first ADCP layer around 1 m from bottom) and C_D is equal to 0.0013.

[31] To characterize the momentum balance, the different terms have been estimated considering three characteristic

Figure 7. (a) Stick plot of measured wind; (b) filtered time series of along-shelf wind (positive is northeastward wind stress); (c) along-shelf sea level gradient (positive means upslope toward northeast); and (d) along-shore depth-averaged velocities for A1, A2 and A3. The solid vertical line corresponds to March 17 (CTD1 measurements). The episodes selected for the momentum balance estimation are shown in the bottom of Figure 7d. (E1 corresponds to storm peak of 12 March; E2 to 19–21 March and E3 to 16–17 April.) Each bar with different color corresponds to different regimes discussed in the text.

episodes that correspond to the dynamic regimes found in section 4.1. Episode 1 (E1) corresponds to strong northeasterly winds (storm event) that generate a negative sea level gradient during 12–15 March (Figure 7). The second analyzed episode (E2) is associated with remote forcing caused by sea level slope during weak wind conditions between March 19 and March 21. Finally, a third episode (E3) corresponds to along-shelf southwesterly winds that drive water toward the northeast between April 16 and April 17. The first order statistics of each term in the along-shelf momentum equation are presented in Table 2 for the A2 location, assuming that the momentum terms are comparable for all ADCPs during the events analyzed.

[32] During the E1 event all of the momentum terms are significant except the baroclinic term. The event is composed of two northeasterly energetic wind peaks intercalated by one period of moderate southwesterly winds (see Figure 7). During the entire event, the dominant terms are the wind stress counteracted by the acceleration and the pressure gradient. The sign of this pressure gradient is consistent with the expected piling of water against the coast, with higher water levels in the ADCP station than in the north sea level gauge (Blanes Harbor). The sea level measurements at Blanes suggest there are uncertainties in the term estimation caused by the location of the sea level gauge within the harbor especially during storms. During the energetic peak, the instantaneous balance is between the pressure gradient and the wind stress (Table 2). The closure of the balance would come from the nonlinear terms, as its magnitudes are consistent with the residual term calculated during this episode.

[33] During episode E2 the first order balance is between the pressure gradient term and acceleration with a secondary contribution from Coriolis and bottom stress. To balance the momentum equation, a small influence of the nonlinear terms is suggested for this episode because the residual term is smaller (0.29 m s^{-2}) than the estimated nonlinear terms. Therefore, this episode corresponds to a balance between pressure gradient and acceleration which has been reported during low wind stress conditions [*Hickey*, 1984].The balance established during episode E3 is given by the acceleration term and the wind stress with a considerable influence of Coriolis acceleration. A secondary role is played by the pressure gradient term and the baroclinic term estimated using the CTD2 measurements. The bottom stress term is small due to the vertical shear of the flow during that episode. This suggests that southwesterly winds acting for a relatively short period are not able to break strong stratification, thus preventing the establishment of a frictional balance between wind and bottom stresses. The increased Coriolis term in E3 is consistent with a divergence of the depth-averaged alongshore currents between the two ADCP located at 25 m (A1 and A2), with velocities at A1 being larger than at A2 (Figure 7). To balance this divergence, an increase in the cross-shelf velocities is expected, resulting in larger Coriolis term. These results are similar to other stratified environment studies [*Lentz*, 2001; *Kirincich et al.*, 2005], which found an increase in cross-shelf Ekman transport in the presence of stratification.

[34] Consequently, the previous analysis suggests that local flow variability can be interpreted using the momentum balance. Different terms play distinctive roles in the equation as a function of the event. For instance, the bottom friction size is different for episodes E1 and E3. In consequence, the analysis of the momentum balance terms complements the dynamic patterns described previously based in statistical formulations. Although the estimation of the pressure gradient term has been done in a spatial scale comparable to the Rossby External Radius, smaller effects associated with spatial atmospheric pressure and wind gradients (feasible in an area with valleys and mountain formations near the shoreline such as the Catalan coast) can influence the local pressure gradient and, in turn, the momentum balance.

[35] Our study area is part of the Mediterranean micro-tidal environment and is under the influence of relatively mild winds resulting in strong stratification [*Font*, 1990]. This causes significant differences in the momentum balance from previously published studies associated with more energetic areas (for instance, *Lee et al.* [1984] in the Mid-Atlantic Bight, USA; *Lentz* [1994] in North Carolina, USA; *Sánchez et al.* [2006] over the Portuguese Shelf; *Fewings and Lentz* [2010] in Martha's Vineyard, USA). Although the importance of the local wind and pressure gradient terms in the momentum balance is obvious, the importance of the bottom stress is observed to be dramatically in the late (warmer) periods (e.g., E3). This deficit is counteracted by an increase in the Coriolis term (Table 2), which leads to more effective Ekman transport. The enhanced stratification resulted in a nearly two-layer water column and promoted a cross-shore transfer of momentum. As a result, the Coriolis term during E3 (estimated to be -1.24 m·s^{-2}) is larger than during E1 and E2 (~ -0.12 and -0.65 m·s^{-2} respectively) when presumably the entire water column was less stratified as suggested by the CTD measurements. Probably, this behavior is relevant in micro-tidal regions with mild winds in contrast to more energetic areas associated with well-mixed conditions. The presence of strong pycnoclines or shears leads to more complex along-shore dynamics [*Lentz and Winant*, 1986]. The present results can be compared with areas of similar stratification in the inner-shelf, for instance, the Northern California Shelf [*Lentz*, 1987], even though that shelf is not micro-tidal. The Coriolis term for the Northern California Shelf was relatively small in comparison to the other terms of the momentum balance. The differences between the Catalan and the Californian inner-shelf presumably emanate from the fact that the southern wind events in Catalan Sea are short (less than one day) in comparison to the Northern California Shelf, where the wind regime is more persistent in time. The transfer of momentum to the bottom requires a certain wind persistency and as the south wind pulses are short over the Catalan shelf, the resulting importance of the Coriolis term is larger as the frictional balance is never fully established. An interpretation of the balance between wind work and heat flux that determine stratification is conducted in the following subsection.

4.3. Vertical Shear, Stratification and River Influence

[36] The effect of stratification is not only related to the momentum balance equation, but also influences the vertical structure of the flow, where a noticeable vertical shear in the along-shelf component is observed (Table 1). Evidences of stratification are also observed in the first and second mode of the EOF analysis and are consistent with the observed shear in the measurements. The stratification is the result of a combination of weak/moderate winds (typical during spring [*Font*, 1990]) and the effective heating due to the

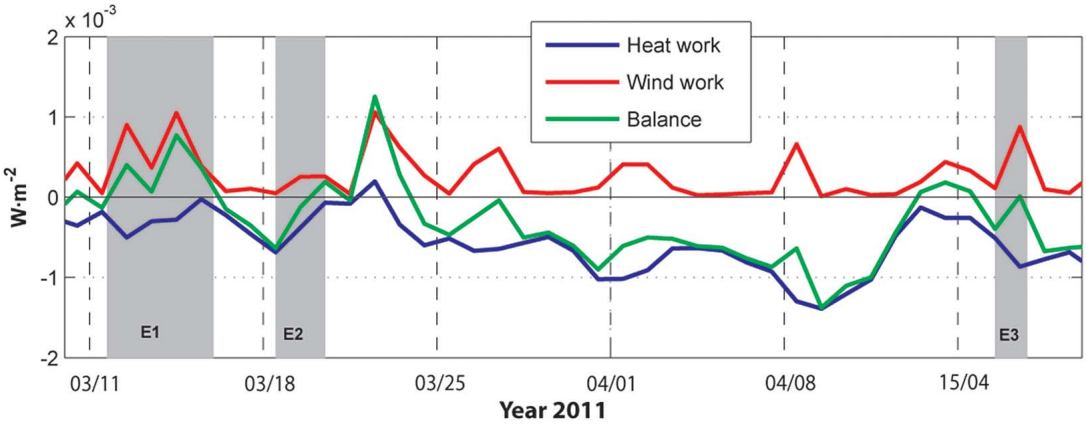

Figure 8. Potential energy changes as a balance of wind and heat work. The gray background indicates the specific episodes analyzed in the momentum balance.

shallowness of the inner-shelf. The stratification during spring is also observed comparing CTD2 against CTD1. The buoyancy frequency is low (~0.002 s^{-1}) and fairly constant below the subsurface layer during CTD1, which indicates a reduced stratification in depth (Figure 4). Conversely, the buoyancy frequency during CTD2 exhibits stronger stratification in the subsurface layers (~0.03 s^{-1}). This is consistent with the reversal depth appreciated in the second EOF mode with a surface layer extending to 5 to 10 m.

[37] Due to the noticeable stratification effects in the vertical shear and, in turn, in the momentum balance, the evolution of the density stratification in the period of analysis is explored using energy formulation. In midlatitudes and in the absence of tidal stirring, the vertical density stratification dynamics can be inferred evaluating the balance of the buoyant forces (basically given by the surface heat flux with a contribution of the freshwater flux) and the mixing forces (essentially the wind energy). In these regions, the incoming solar radiation presents an annual cycle with variability much larger than those presented by mechanisms with smaller time-scales. To assess the water column changes during March and April 2011, the energy input to create stratification is compared with the mixing energy to destroy it. Following the classical methodology suggested by *Simpson and Bowers* [1981], the potential energy (PE) is defined as:

$$PE = \int_{-h}^{0} \beta = \frac{1}{\rho_0} \int_{-h}^{0} (\rho - \rho_0) g \cdot z \cdot dz \qquad (4)$$

where β is the buoyancy per unit volume. Positive inputs of PE occur through wind mixing and negative from heat fluxes. In consequence, neglecting horizontal advection, tidal mixing and wave action contributions, the balance is between surface heat flux buoyancy effects and wind mixing. Thus, the change of Potential Energy (PE) is computed as:

$$\frac{\partial PE}{\partial t} = -\frac{\alpha g Q H}{2 C_p} + \varepsilon_s \rho_a \gamma C_{Ds} W_{10}^3 \qquad (5)$$

where C_p is the specific heat of seawater at constant pressure (4×10^3 $Jkg^{-1}C^{-1}$), Q is the surface heat flux, H is the water depth, α thermal expansion coefficient, ε_s is the wind mixing efficiency, C_{DS} is the surface drag coefficient, ρ_a is the air density, γ is the ratio of the wind-induced surface current to the wind speed and W is the wind velocity. The wind mixing efficiency is assumed to be 0.03 following *Atkinson and Blanton* [1986]. The surface heat flux (W m^{-2}) is obtained from the European Centre for Medium-range Weather Forecast (ECMWF, www.ecmwf.int) products in daily frequency. The mixing work due to the wind is obtained from the wind observations in the study area interpolated to one-day intervals. The main limitation of the analysis is that the value of the potential energy is unknown because of the lack of vertical density time series.

[38] The balance between the heat stratification contribution and the wind mixing for the period of analysis suggests that conditions favoring stratification tend to be predominant (Figure 8). A negative balance (tendency to increase stratification) between both terms is observed except for a few short periods when a reverse behavior is estimated. Basically, the heat flux contribution is between 2 and 3 times larger than wind mixing. Several peaks are observed in the balance, which are associated with energetic wind events. In particular, the storm event between 12 and 15 March (E1) results in a positive energy balance suggesting a tendency toward mixing conditions consistent with buoyancy frequency values under the sub-surface layer during CTD1. Mixed conditions might be prevented due to the presence of freshwater from the river plume contribution in particular in the surface layers (Figure 3f). During the rest of the study period, a negative balance is observed, where presumably the pressure gradient (E2) and the short wind events (e.g., wind period during April 9) cannot completely mix the water column. Only a reduction in the value of the heat flux (e.g., E3), combined with wind pulses can achieve positive values in the balance providing a tendency to mix the water column. As the potential energy balance has been predominantly controlled by stratification, it is unlikely that wind can mix the entire water column except in areas where wave action is also a factor (i.e., near the surf zone).

[39] The influence of freshwater discharge from the Besòs River during flash flood (12–15 March) is not clearly observed in the velocity time series (March 17, solid vertical line in Figure 7). During that period, the flow associated with river discharge through density driven modifications is expected to be small in the inner-shelf, and probably only

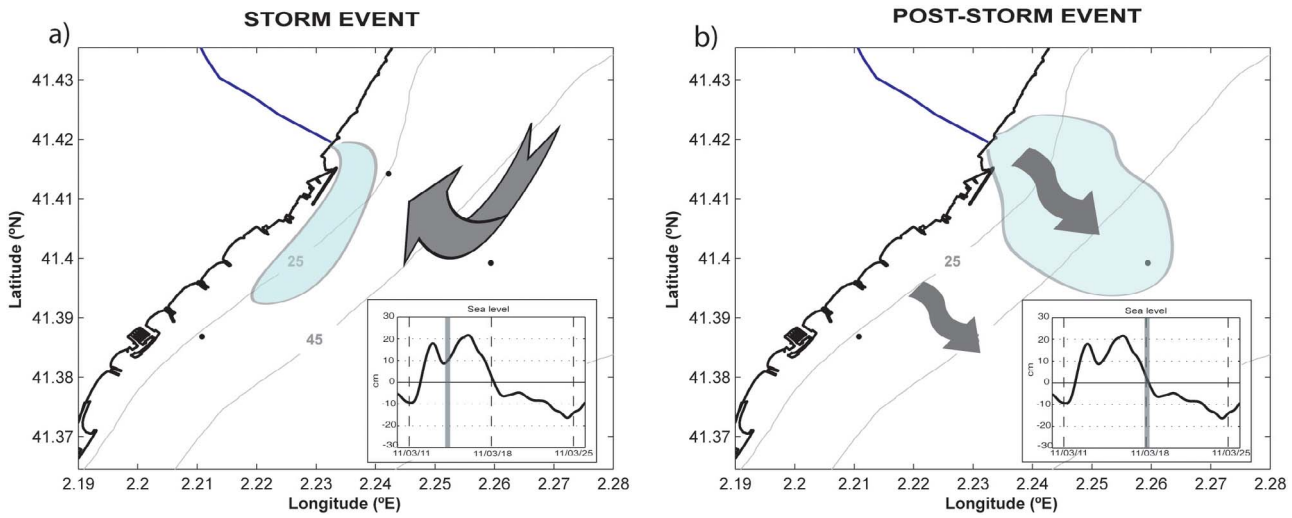

Figure 9. (a) Idealized flow behavior and river plume response (in blue) during the storm event (northeasterly winds) and (b) during the post-storm or relaxation period with simplified salinity field observed during CTD1. The inset figure is the sea level measured at the Coastal Station Observatory showing the corresponding time with vertical gray bars.

noticeable in a limited area near the Besòs River mouth. Furthermore, a distinct hydrographic structure is evident from CTD1 (post-rain conditions) in the salinity measurements (Figure 3d). A signal of the detached plume is observable offshore southeast of the river mouth and extending at least to the 60 m isobath. The CTD casts of March 17 were collected two days after the river discharge peak (Figure 3a). The sharp peak is associated with the 12–15 March storm event. During that period, the northeasterly wind piles the water against the coast (downwelling favorable winds), consistent with observed sea level increase. Presumably, the plume is trapped in the shallowest areas due to the Coriolis effect. An idealized plume response is shown in the Figure 9 as well as the sea level time series for the mentioned period. After the storm, during calm wind conditions, a relaxation of the sea level is observed (Figure 9b). During that time, the sea level decreases and the surface cross-shelf flow is offshore pushing the surface freshwater cell from the River mouth offshore. The progressive vector diagram (Figure 10) shows southwestward flow during 16 March (late storm conditions) followed by northeastward surface velocity during March 17 at the time of the CTD surveys (relaxation period). The flash-flood character of the river discharge and the shallowness of the inner-shelf result in a rapid plume evolution during and after downwelling favorable winds. In consequence, a fast river plume response is expected consistently with the water column response to the wind. The exceptionality of the river discharge flow preceding CTD1 measurements suggests considering these hydrographic conditions as sporadic, while the CTD2 conditions fields are more representative of normal temperature and salinity fields.

5. Conclusions and Future Work

[40] The along-shelf current fluctuations in the inner Catalan shelf during spring are mainly controlled by local wind stress in short time scales and remotely by sea level gradients in synoptic time scales. As might be expected, the importance of the local wind is intensified by the shallowness of the area studied. Except for specific events during storm periods, the measured sea level slope is remotely generated by large-scale pressure gradients, not as a direct response to local wind. Additional forcing mechanisms are involved in the along-shelf momentum balance (e.g., baroclinic term, bottom stress) and the flow responds differently (variable importance of the nonlinear terms and Coriolis acceleration) during specific events. The vertical structure of the velocity is mainly controlled by the vertical density gradient with a smaller contribution of frictional effects. The vertical shear in velocity is accompanied by the development of stratified conditions

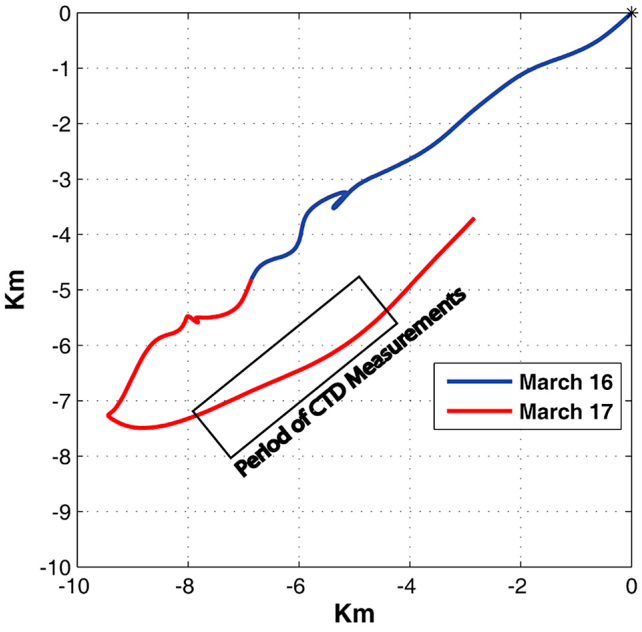

Figure 10. Progressive vector diagram of the current in A1 during 16 and 17 March for the near-surface ADCP bin.

caused by heating that the typical wind is not able to counteract according to the potential energy balance. The presented momentum balance differs from the results from other studies that were conducted in tidally dominated regions that tend to be more energetic. In our case, the stratification alters the sizes of the momentum terms with a decrease importance of bottom stress and an increase relevance of the Coriolis acceleration. Finally, a short time response to the Besòs plume influence (hours to days) is observed, caused by the shallowness of the plume evolution, the rapid pulse of river discharge and the relaxation of cross-shore velocities after a storm event.

[41] The observed importance of the pressure gradient in the along-shore flow suggests that determining the presence and magnitude of coastally trapped waves might be necessary to characterize the velocity fluctuations if they behave similarly to other coastal domains [*Hickey*, 1984]. The internal deformation radius, using averaged buoyancy frequencies, is estimated to be around 10 km in the study area, suggesting the internal wave activity should be trapped in an area covering a significant portion of the shelf. A future study focusing on the propagation of coastal trapped waves over the Catalan inner-shelf might be of interest to complement similar analysis over deeper waters in the Northwestern Mediterranean Sea [*Jordi et al.*, 2005].

[42] The estimation of the nonlinear terms and other local dynamics (e.g., wave action effects) are still not completely resolved. Additional observational campaigns, covering the surf zone and the mid-shelf, and the investigation of cross-shelf dynamics or river plume evolution are tasks of importance in an area with strong anthropogenic impacts (i.e., Barcelona city hinterland). Finally, the results presented here will support future studies focused on the management and investigation of the coastal and shelf area (e.g., environmental concerns, water quality degradation, sediment transport dynamics) and establish a framework for the interpretation of process-oriented and operational model simulations.

[43] This contribution provides a first interpretation of the inner-shelf dynamics in the Catalan Sea and is limited to the period of observation. Further work should focus on the effect of the annual cycle of heat flux and wind energy on the flow vertical structure.

[44] **Acknowledgments.** The authors would like to acknowledge Anthony Kirincich (WHOI, Woods Hole), and Steve Lentz (WHOI, Woods Hole) for their comments and suggestions. Josep Lluís Pelegrí of the Institut de Ciències del Mar (ICM/CSIC, Barcelona) reviewed an early version of the manuscript and provided helpful comments. The authors are thankful for the helpful suggestions from two anonymous reviewers and from Ilgar Safak (USGS, Woods Hole) and Neil Ganju (USGS, Woods Hole) that helped to improve the quality of the manuscript. Thanks also to the technical staff of LIM/UPC: Joan Puigdefàbregas and Jordi Cateura for the data acquisition and Cesar Mosso and Marc Mestres for the data pre-processing. The research leading to these results has received funding from the European Community's Seventh Framework Programme (FP7/2007/2013) under grant agreement 242284 (Field_ac project).

References

Allen, J. S., and P. K. Kundu (1978), On the momentum, vorticity and mass balance on the Oregon Shelf, *J. Phys. Oceanogr.*, *8*(1), 13–27, doi:10.1175/1520-0485(1978)008<0013:OTMVAM>2.0.CO;2.

Atkinson, L. P., and J. O. Blanton (1986), Processes that affect stratification in the shelf waters, in *Baroclinic Processes on Continental Shelves*, *Coastal Estuarine Sci.*, vol. 3, edited by C. N. K. Mooers, pp. 117–130, AGU, Washington, D. C., doi:10.1029/CO003p0117.

Bourrin, F., P. L. Friend, C. L. Amos, E. Manca, C. Ulses, A. Palanques, X. Durrieu de Madron, and C. E. L. Thompson (2008), Sediment dispersal from a typical Mediterranean flood: The Têt River, Gulf of Lions, *Cont. Shelf Res.*, *28*(15), 1895–1910, doi:10.1016/j.csr.2008.06.005.

Fewings, M. R., and S. J. Lentz (2010), Momentum balances on the inner continental shelf at Martha's Vineyard Coastal Observatory, *J. Geophys. Res.*, *115*, C12023, doi:10.1029/2009JC005578.

Font, J. (1990), A comparison of seasonal winds with currents on the continental slope of the Catalan Sea (northwestern Mediterranean), *J. Geophys. Res.*, *95*(C2), 1537–1545, doi:10.1029/JC095iC02p01537.

Hickey, B. M. (1984), The fluctuating longshore pressure gradient on the Pacific Northwest shelf: A dynamical analysis, *J. Phys. Oceanogr.*, *14*(2), 276–293, doi:10.1175/1520-0485(1984)014<0276:TFLPGO>2.0.CO;2.

Jordà, G., and P. De Mey (2010), Characterization of error dynamics in a 3D coastal model of the Catalan sea using stochastic modelling, *Cont. Shelf Res.*, *30*(5), 419–441, doi:10.1016/j.csr.2009.12.013.

Jordi, A., A. Orfila, G. Basterretxea, and J. Tintoré (2005), Coastal trapped waves in the northwestern Mediterranean, *Cont. Shelf Res.*, *25*(2), 185–196, doi:10.1016/j.csr.2004.09.012.

Kirincich, A. R., and J. A. Barth (2009), Alongshelf variability of inner-shelf circulation along the central Oregon coast during summer, *J. Phys. Oceanogr.*, *39*(6), 1380–1398, doi:10.1175/2008JPO3760.1.

Kirincich, A. R., J. Barth, B. A. Grantham, B. A. Menge, and J. Lubchenco (2005), Wind-driven inner-shelf circulation off central Oregon during summer, *J. Geophys. Res.*, *110*, C10S03, doi:10.1029/2004JC002611.

Large, W. G., and S. Pond (1981), Open ocean momentum flux measurements in moderate to strong winds, *J. Phys. Oceanogr.*, *11*(3), 324–336, doi:10.1175/1520-0485(1981)011<0324:OOMFMI>2.0.CO;2.

Lee, T. N., W. J. Ho, V. Kourafalou, and J. D. Wang (1984), Circulation on the continental shelf of the southeastern United States. Part I: Subtidal response to wind and gulf stream forcing during winter, *J. Phys. Oceanogr.*, *14*(6), 1001–1012, doi:10.1175/1520-0485(1984)014<1001:COTCSO>2.0.CO;2.

Lentz, S. J. (1987), A description of the 1981 and 1982 spring transitions over the northern California shelf, *J. Geophys. Res.*, *92*(C2), 1545–1567, doi:10.1029/JC092iC02p01545.

Lentz, S. J. (1994), Current dynamics over the northern California inner shelf, *J. Phys. Oceanogr.*, *24*(12), 2461–2478, doi:10.1175/1520-0485(1994)024<2461:CDOTNC>2.0.CO;2.

Lentz, S. J. (2001), The influence of stratification on the wind-driven cross-shelf circulation over the North Carolina shelf, *J. Phys. Oceanogr.*, *31*, 2749–2760, doi:10.1175/1520-0485(2001)031<2749:TIOSOT>2.0.CO;2.

Lentz, S. J., and D. C. Chapman (2004), The importance of nonlinear cross-shelf momentum flux during wind-driven coastal upwelling, *J. Phys. Oceanogr.*, *34*(11), 2444–2457, doi:10.1175/JPO2644.1.

Lentz, S. J., and C. D. Winant (1986), Subinertial currents on the southern California shelf, *J. Phys. Oceanogr.*, *16*(11), 1737–1750, doi:10.1175/1520-0485(1986)016<1737:SCOTSC>2.0.CO;2.

Lentz, S., R. T. Guza, S. Elgar, F. Feddersen, and T. H. C. Herbers (1999), Momentum balances on the North Carolina inner shelf, *J. Geophys. Res.*, *104*(C8), 18,205–18,226, doi:10.1029/1999JC900101.

Li, Z., and R. H. Weisberg (1999), West Florida continental shelf response to upwelling favorable wind forcing: 2. Dynamics, *J. Geophys. Res.*, *104*(C10), 23,427–23,442, doi:10.1029/1999JC900205.

Liu, Y., and R. H. Weisberg (2005), Momentum balance diagnoses for the West Florida Shelf, *Cont. Shelf Res.*, *25*(17), 2054–2074, doi:10.1016/j.csr.2005.03.004.

Millot, C. (1999), Circulation in the western Mediterranean Sea, *J. Mar. Syst.*, *20*(1–4), 423–442, doi:10.1016/S0924-7963(98)00078-5.

Pettigrew, N. R., and S. P. Murray (1986), The coastal boundary layer and inner shelf, in *Baroclinic Processes on Continental Shelves*, *Coastal Estuarine Sci.*, vol. 3, edited by C. N. K. Mooers, pp. 95–108, AGU, Washington, D. C., doi:10.1029/CO003p0095.

Rippeth, T. P., J. H. Simpson, R. J. Player, and M. Garcia (2002), Current oscillations in the diurnal–inertial band on the Catalonian shelf in spring, *Cont. Shelf Res.*, *22*(2), 247–265, doi:10.1016/S0278-4343(01)00056-5.

Rubio, A., P. A. Arnau, M. Espino, M. del Mar Flexas, G. Jordà, J. Salat, J. Puigdefàbregas, and A. S. Arcilla (2005), A field study of the behaviour of an anticyclonic eddy on the Catalan continental shelf (NW Mediterranean), *Prog. Oceanogr.*, *66*(2–4), 142–156, doi:10.1016/j.pocean.2004.07.012.

Salat, J., J. Tintore, J. Font, D.-P. Wang, and M. Vieira (1992), Near-inertial motion on the shelf-slope front off northeast Spain, *J. Geophys. Res.*, *97*(C5), 7277–7281, doi:10.1029/92JC00588.

Salat, J., et al. (2002), Seasonal changes mass structure and shelf slope at the Ebre Shelf (NW Mediterranean), *Cont. Shelf Res.*, *22*, 327–348, doi:10.1016/S0278-4343(01)00031-0.

Sánchez, R. F., E. Mason, P. Relvas, A. J. da Silva, and Á. Peliz (2006), On the inner-shelf circulation in the northern Gulf of Cádiz, southern Portuguese

shelf, *Deep Sea Res., Part II*, *53*(11–13), 1198–1218, doi:10.1016/j.dsr2.2006.04.002.

Sánchez-Arcilla, A., and J. H. Simpson (2002), The narrow shelf concept: Couplings and fluxes, *Cont. Shelf Res.*, *22*(2), 153–172, doi:10.1016/S0278-4343(01)00052-8.

Simpson, J. H., and D. Bowers (1981), Models of stratification and frontal movement in shelf seas, *Deep Sea Res., Part A*, *28*(7), 727–738, doi:10.1016/0198-0149(81)90132-1.

Tonani, M., N. Pinardi, C. Fratianni, J. Pistoia, S. Dobricic, S. Pensieri, M. de Alfonso, and K. Nittis (2009), Mediterranean Forecasting System: Forecast and analysis assessment through skill scores, *Ocean Science*, *5*(4), 649–660, doi:10.5194/os-5-649-2009.

Winant, C. D., and R. C. Beardsley (1979), A comparison of some shallow wind-driven currents, *J. Phys. Oceanogr.*, *9*(1), 218–220, doi:10.1175/1520-0485(1979)009<0218:ACOSSW>2.0.CO;2.

Winant, C. D., and A. W. Bratkovich (1981), Temperature and currents on the Southern California Shelf: A description of the variability, *J. Phys. Oceanogr.*, *11*, 71–86, doi:10.1175/1520-0485(1981)011<0071:TACOTS>2.0.CO;2.